Tai *et al. Chem Synth* 2023;3:38
DOI: 10.20517/cs.2023.27

Chemical Synthesis

Research Article

Open Access

A simple strategy for synthesis of *b*-axis-oriented MFI zeolite macro-nanosheets

Wenshu Tai[1], Weijiong Dai[1], Guangjun Wu[1,2,*], Landong Li[1,2,*]

[1]School of Materials Science and Engineering, Nankai University, Tianjin 300350, China.
[2]College of Chemistry, Nankai University, Tianjin 300071, China.

[*]**Correspondence to:** Prof. Guangjun Wu, Prof. Landong Li, College of Chemistry, Nankai University, Weijin Road 94, Nankai District, Tianjin 300071, China. E-mail: wuguangjun@nankai.edu.cn; lild@nankai.edu.cn

How to cite this article: Tai W, Dai W, Wu G, Li L. A simple strategy for synthesis of *b*-axis-oriented MFI zeolite macro-nanosheets. *Chem Synth* 2023;3:38. https://dx.doi.org/10.20517/cs.2023.27

Received: 12 May 2023 **First Decision:** 29 Jun 2023 **Revised:** 27 Jul 2023 **Accepted:** 14 Aug 2023 **Published:** 25 Aug 2023

Academic Editors: Bao-Lian Su, Jun Xu, Aicheng Chen **Copy Editor:** Pei-Yun Wang **Production Editor:** Pei-Yun Wang

Abstract

Zeolite nanosheets with shortened diffusion paths and high external surface areas have drawn significant attention. This unique morphology of zeolites can endow them with reduced diffusion resistance and high accessibility of active sites, and thereby good catalytic performance. Exploring simple synthesis strategies for zeolite nanosheets is mostly desired in zeolite chemistry. Herein, MFI zeolite nanosheets with a thickness of 50-100 nm along the *b*-axis and a length of 1 μm along the *c*-axis, namely zeolite macro-nanosheets, have been successfully synthesized *via* the strategy of combining pre-aging and pH regulation without the use of complex templates/additives and fluorine media. Pre-aging at a relatively high temperature of 90 °C and low alkalinity for crystallization (pH = 7.0~8.5) are found to play key roles in controlling macro-nanosheet synthesis, which can promote the formation of MFI zeolite precursors and then dissociate them into smaller ones for the following oriented aggregation during hydrothermal treatment. Crystallization kinetic studies suggest that the two-dimensional crystal growth is the intrinsic behavior of zeolite crystallization under employed conditions. This synthesis strategy can be easily extended to the synthesis of heteroatom-containing MFI macro-nanosheets, such as ZSM-5 and TS-1.

Keywords: MFI zeolite, macro-nanosheets, per-aging, pH regulation, crystallization mechanism

INTRODUCTION

Zeolites have been widely used in catalysis, separation, and ion exchange due to their crystalline framework,

special composition of Si and Al, high thermal/hydrothermal stability, and especially the unique microporous structure, which endows zeolites with fascinating shape selectivity. However, such micropores on a molecular scale (generally < 1 nm) also cause serious diffusion problems, limiting the application of zeolites when dealing with bulky molecules[1,2]. Among the solutions, constructing zeolite nanosheets has attracted great attention and emerged as a hot topic in zeolite chemistry over the past decades.

A key breakthrough in the synthesis of zeolite nanosheets was achieved by Choi *et al.*[3,4]. Therein, MFI zeolite nanosheets with a single-unit-cell thickness along the *b*-axis were synthesized by using a specially designed di-quaternary ammonium-type surfactant as a structure-directing agent (SDA), which owns hydrophobic alkyl chains limiting zeolite crystal growth along certain direction. Subsequently, Xu *et al.* explored a new type of special SDAs with aromatic groups to synthesize MFI nanosheets with house-of-cards[5] and two-dimensional (2D) square arrangements[6]. Mordenite (MOR) zeolite nanosheet has also been synthesized by this type of special SDAs[7]. However, these SDAs were deliberately designed and thus costly, limiting their large-scale applications. Theoretically, each zeolite nanosheet could be synthesized if growth in the third dimension can be efficiently suppressed[8], especially for zeolites with non-layered structures, such as MFI zeolites, which are considered as the second most important zeolite in catalysis after the FCC catalysts of FAU zeolites[9]. Crystal growth modifiers have already been explored for synthesis of zeolite nanosheets, for example, urea[10-14], diols[15], spermine and tributylphosphine oxide[16], L-carnitine[17], ethanol[18], and guanidine[19,20]. Among them, urea is mostly used due to its low cost and ready availability. With the help of the above modifiers, MFI zeolite nanosheets with a thickness of 50~300 nm along the *b*-axis direction can be obtained.

An alternative protocol is synthesizing self-pillared pentasil (SPP) zeolite nanosheets with small SDAs by intergrowth of MFI and MEL zeolites. Zhang *et al.* reported the synthesis of SPP zeolite nanosheets by repetitive branching, which resulted in the intergrowth in a house-of-cards arrangement of nanosheets with a thickness of 2 nm[21]. Recently, Ma *et al.* developed a series of pyridine-based cations as templates for rational synthesis of SPP zeolite nanosheets, possessing house-of-cards morphology and excellent hydrothermal stability and exhibiting superior catalytic performance in the methanol-to-propylene reaction[22]. Notably, Al-rich SPP zeolite nanosheets have been synthesized under SDA-free methods by using MEL or MFI seeds to induce spontaneous formation[23]. On the other hand, besides bottom-up synthesis, the zeolite nanosheets can be prepared via a top-down anisotropic etching strategy in an aqueous solution of organic alkaline, and the thicknesses of the as-prepared silicalite-1 and ZSM-5 nanosheets can be as thick as 10 and 100 nm, respectively[24,25].

The space between zeolite nanosheets with a thickness of several nanometers could be greatly reduced after removing the SDAs by calcination[1]. Meanwhile, the ultrathin nanosheets can cause a decline in stability and high cost in separation and purification. In our previous work[26], a simple synthesis strategy for platelike MFI zeolites in fluorine media has been developed. The obtained platelike MFI zeolites, denoted as MFI zeolite macro-nanosheets (ZMNs), own a thickness of 10~100 nm along the *b*-axis and size in micrometer-range along *a*- and *c*-axes and an extra high aspect ratio of L_c/L_b = 25, resulting in shortened diffusion path and easy separation from the synthesis mother liquid. The synthesis strategy is effective and versatile and can be used for the synthesis of other ZMNs[27-30]. Very recently, a similar strategy combining seed suspension and fluoride cooperation in a near-neutral gel system has been reported for the synthesized MFI ZMNs with thicknesses lower than 50 nm[31-33]. However, fluoride is generally required for the synthesis of ZMNs, which is quite harmful to the environment[34]. Herein, a simple environmental-friendly strategy for synthesis of MFI ZMNs is reported by combining the pre-aging and pH regulation without using complex SDAs/additives or fluoride. The effects of pre-aging and pH regulation are investigated in detail,

and the crystallization process is monitored by microscopy and spectroscopy. Heteroatom-containing MFI ZMNs, namely ZSM-5 and TS-1 ZMNs, can also be successfully synthesized via the presented strategy.

RESULTS AND DISCUSSION

MFI (silicalite-1, S-1) ZMNs were synthesized by aging the gel with a molar composition of 1.0 SiO_2 : 0.15 Tetrapropylammonium hydroxide (TPAOH) : 25 H_2O at 90 °C for 12 h, followed by regulating the pH of aging gel to 8.5 and aging for another 12 h, and then crystallization at 120 °C for 72 h. The X-ray diffraction (XRD) patterns, Ar adsorption-desorption isotherms, and representative scanning electron microscope (SEM) and transmission electron microscopy (TEM) images of the as-synthesized S-1 ZMNs are presented in Figure 1. Obviously, the S-1 ZMNs show typical diffraction peaks of MFI structures with high relative crystallinity (~94% with commercial ZSM-5 zeolites as a reference) [Figure 1A] and hexagonal nanosheet morphology with dimensions of ~250 nm, ~80 nm, and ~800 nm along the *a*-, *b*-, and *c*-axes, respectively [Figure 1C and D], presenting aspect ratios of ~3 for L_a/L_b and ~10 for L_c/L_b. The type I Ar adsorption-desorption isotherms and pore size distribution confirm the microporous structure of ZMNs with a micropore volume of 0.134 cm^3/g and a specific surface area of 426 m^2/g [Supplementary Table 1]. The high crystallinity of the S-1 ZMNs can also be demonstrated by the well-aligned lattice fringes in the high-resolution TEM image [Figure 1E] and the corresponding selected area electron diffraction (SAED) pattern [Figure 1F].

The process of aging is critical in the production of zeolites as it can enhance the nucleation rate and shorten the nucleation period[35]. Therefore, prolonged aging time can generate precursors similar to the final product, thereby further shortening the crystallization time. In our previous work, the aging process is demonstrated to be necessary for the synthesis of MFI ZMNs in fluoride media[26]. Here, the effect of aging on S-1 ZMN synthesis is first investigated. As shown in Supplementary Figures 1 and 2, without the aging step, the solid sample appears to be amorphous after 72 h, while it can crystallize after 120 h with relatively low crystallinity, indicating the promoted crystallization by aging treatment. However, in this case, the obtained sample presents twin crystal morphology instead of macro-nanosheet morphology [Supplementary Figure 2A]. Prolonging the aging time from 12 to 36 and 72 h, the crystallization time can be significantly shortened from 72 to 48 and 24 h to achieve similar crystallinity with the ZMNs. However, the obtained samples lose their nanosheet morphology and present coffin morphology as traditional bulky MFI zeolites, although the size along the *b*-axis was about 100 nm (*ca.* 1~2 for L_a/L_b and 2~4 for L_c/L_b). These observations confirm the promotion effect of the aging process on crystallization, and appropriate aging time is necessary for S-1 ZMN synthesis.

The effect of aging temperature is then explored, as shown in Supplementary Figure 3. Twin crystals are obtained when the aging step is performed at 30 and 50 °C, while single nanosheet crystals are obtained if the aging temperature is raised to 70 and 90 °C. The sizes of obtained MFI crystals differ significantly in all three orientations; namely, the samples synthesized at low aging temperatures are thicker and larger than those at 90 °C. Fourier transform infrared (FTIR) is employed to illustrate the state of the aging gel, as shown in Supplementary Figure 4. A broad band at 570 cm^{-1} assignable to the vibration of a typical five-membered ring (5MR) in pentasil zeolites is clearly observed, which is blue-shifted from 550 cm^{-1} (double 5MR in bulky pentasil zeolites) with decreasing particle size[36]. It is also reported that the band at 570 cm^{-1} was the character of MFI nanoslab particles with a size of 1.3 nm × 4 nm × 4 nm[36] or of young precursor-type particles[37]. That is, the presence of a band at 570 cm^{-1} implies the formation of small MFI precursors (crystal nucleus) in the aging gel, although the XRD patterns indicate the amorphous state of the aging gel [Supplementary Figure 5]. This is also supported by the Ar adsorption-desorption isotherms and the pore size distribution of the aging gel, which exhibits type I isotherms and a pore width of 0.7 nm

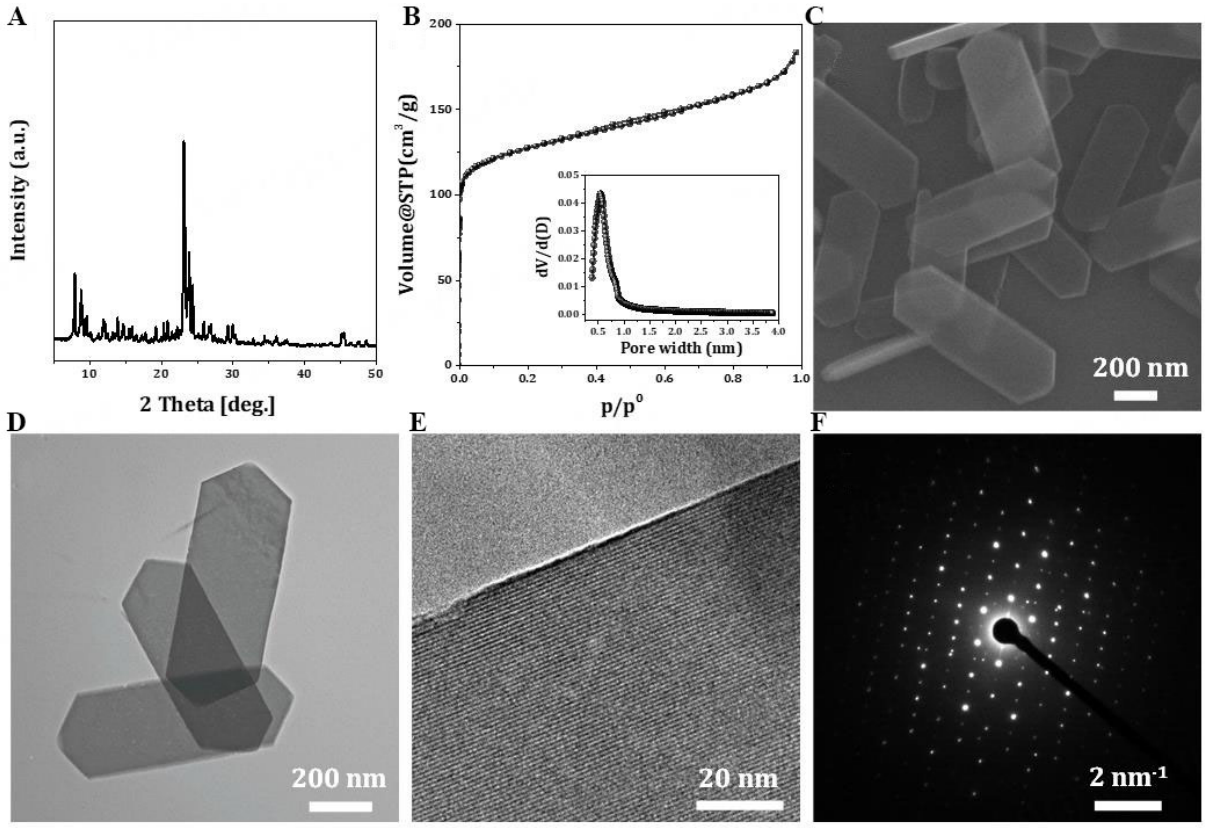

Figure 1. General features of S-1 ZMNs synthesized at an aging temperature of 90 °C for 12 h and crystallization temperature of 120 °C for 72 h (pH = 8.5): (A) XRD patterns; (B) Ar adsorption-desorption isotherms with pore size distribution shown inset; (C) SEM image; (D) TEM and (E) high-resolution TEM images; and (F) SAED patterns. SAED: Selected area electron diffraction; SEM: scanning electron microscope; TEM: transmission electron microscopy; XRD: X-ray diffraction; ZMNs: zeolite macro-nanosheets.

[Supplementary Figure 6], indicating the formation of microporous structures with a certain degree of order. Moreover, the BET surface area, total pore volume, and micropore volume of the aging gel are all higher than those of the as-synthesized S-1 ZMNs, demonstrating again that the aging gel possesses microporous structures and short-range order. Thus, it can be concluded that aging at a relatively high temperature (90 °C) and appropriate time (12 h) plays a crucial role in S-1 ZMN synthesis, which can produce MFI precursors (crystal nucleus) with enough concentration ready for the consequent oriented aggregation and thus deplete the nutrition to reduce the nucleation during hydrothermal treatment as much as possible. Hence, it is speculated that when aging at low temperatures (< 90 °C), the concentration of MFI precursors (crystal nucleus) is not high enough for the oriented aggregation. In this context, the nucleation and crystal growth will occur simultaneously during hydrothermal treatment as the traditional MFI crystallization, producing traditional twin crystals. Prolonging the aging time will make the aging gel enter the crystal growth stage, which is not affected by the pH regulation after aging, as discussed in the following section.

The pH regulation is another crucial factor for S-1 ZMN synthesis. The influence of pH is explored, as shown in Figure 2 and Supplementary Figure 7. The morphology is significantly influenced by the pH of the aging gel: the length along the *c*-axis changes significantly, increasing from *ca.* 400 to 1,600 nm, while the thickness along the *b*-axis becomes slightly thinner from over 100 to 50~80 nm with decreasing pH of the aging gel from 9.5 to 7.0, and the length along the *a*-axis remains almost constant (*ca.* 250 nm).

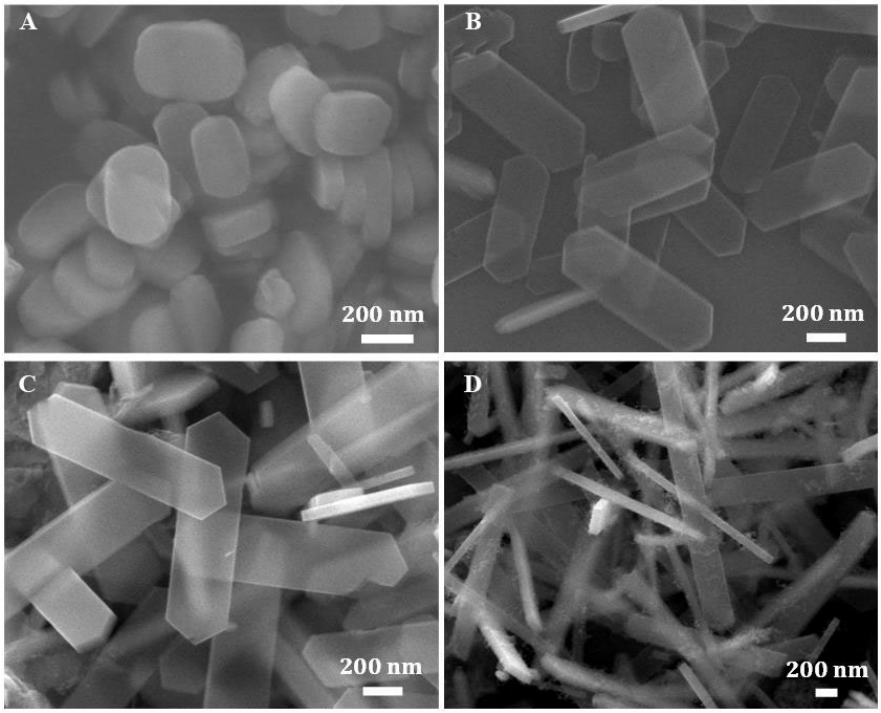

Figure 2. SEM images of S-1 ZMNs synthesized at different pH values of the aging gel and different crystallization times: (A) pH = 9.5, 48 h; (B) pH = 8.5, 72 h; (C) pH = 8.0, 72 h; and (D) pH = 7.0, 168 h. Crystallization temperature: 120 °C (A and B) or 150 °C (C and D). SEM: Scanning electron microscope; ZMNs: zeolite macro-nanosheets.

Interestingly, without pH regulation, the sample synthesized under alkaline conditions (pH = 11.4) presents a length along the *a*- and *c*-axes of 300 nm and a thickness along the *b*-axis of 180 nm [Supplementary Figure 8], displaying typical nano MFI zeolite morphology. It seems that the pH regulation can significantly promote the crystal growth along the *c*-axis, moderately decrease the crystal growth along the *b*-axis, and poorly affect the crystal growth along the *a*-axis; namely, the pH regulation could enhance and/or suppress the growth of different zeolite crystal faces, thereby resulting in the formation of zeolite nanosheets. In other words, decreasing the pH of the aging gel will lead to the formation of the nanosheet crystals due to the enhancement for the oriented aggregation of the MFI precursors (crystal nucleus), as shown in Figure 3. FTIR and Ar adsorption-desorption isotherms are performed to detect the state of the aging gel after pH regulation, as shown in Supplementary Figures 4 and 6, respectively. After regulating the pH of the aging gel to 8.5, the intensity of the band at 570 cm^{-1}, attributed to the small MFI precursors, decreases distinctly, indicating that the MFI precursors are destroyed to some extent or dissociated into tiny particles (or the crystal nuclei is disturbed). This is also suggested by the Ar adsorption-desorption isotherms, which vary from type I to type IV isotherms because of the loss of microporous structures and the aggregation of tiny particles (precursors) [Supplementary Figure 6]. The significant consumption of microporous structures caused by decreasing pH is, therefore, evidenced. The pore size distribution broadens, and the pore width enlarges obviously; meanwhile, the BET surface area drops sharply from 541 to 274 m^2/g, and the microporous volume is completely lost [Supplementary Table 1]. However, it is speculated that the tiny particles (precursors) still own the memory of MFI topology, and they can quickly crystallize during hydrothermal treatment, as their crystallization time is much shorter than that without the aging step.

On the other hand, it is reported that relatively low alkalinity and neutral medium are unfavorable for zeolite nucleation and crystallization, and fluoride ion is usually needed[38]. Indeed, in the present cases, the

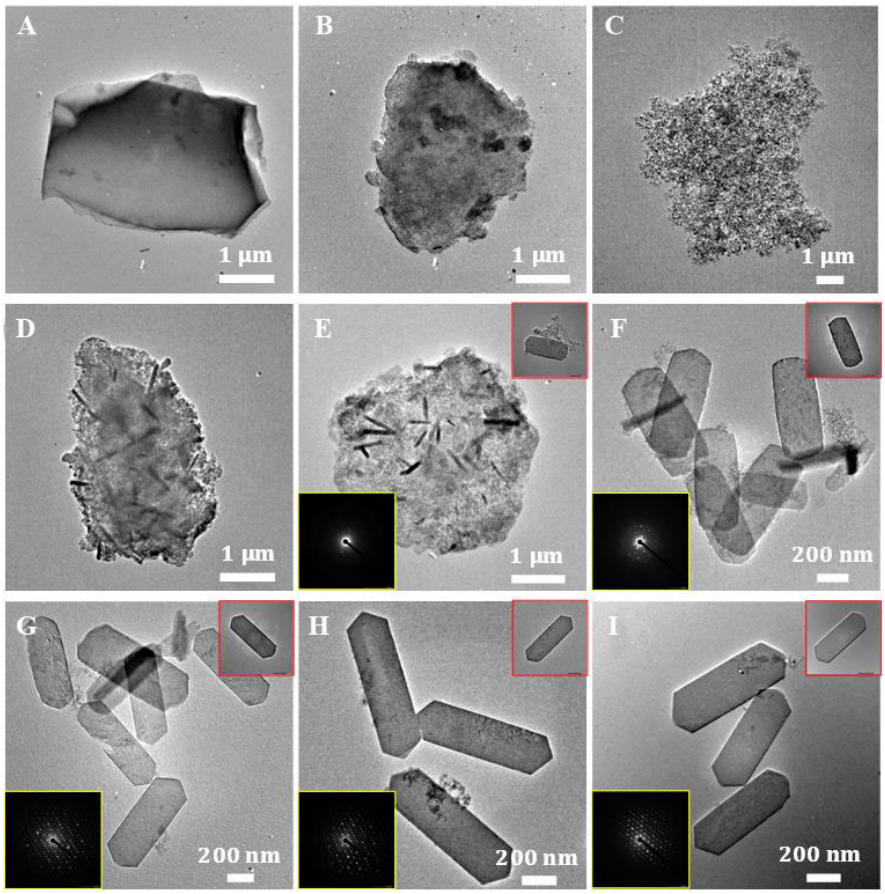

Figure 3. TEM analyses of samples at different stages of S-1 ZMN synthesis: (A) after aging at 90 °C for 12 h; (B) after regulating pH to 8.5 and aging at 90 °C for another 12 h; after hydrothermal treatment in the autoclave at 120 °C for (C) 6; (D) 9; (E) 12; (F) 16; (G) 24; (H) 48; and (I) 72 h. TEM: Transmission electron microscopy; ZMN: zeolite macro-nanosheet.

crystallization time prolongs and the crystallization temperature rises with decreasing the pH to achieve a similar crystallinity, and amorphous species can be observed even after crystallization for 168 h when the pH decreased to 7.0, indicating the strongly suppressing effect of decreasing pH. Nevertheless, S-1 ZMNs have been successfully synthesized with high crystallinity in fluorine-free mediums at pH = 8.5 and pH = 8.0. In contrast, the sample synthesized at pH = 8.5 without aging treatment appears to be amorphous after 72 h [Supplementary Figure 1], and it has even been reported that the material obtained is still amorphous after crystallization at 150 °C for one month when the pH is adjusted to 8.5[39]. Interestingly, the thickness along the *b*-axis of MFI zeolites is still 180 nm when the pH of the synthesis system is ~7.0[40]. These comparisons unambiguously demonstrate the essential role of the aging step for the synthesis of S-1 ZMNs under present conditions, not only for promoting the crystallization but also for the oriented aggregation by combining the subsequent pH regulation.

The effect of various types of acids on the synthesis of S-1 ZMNs is further explored. As shown in Supplementary Figure 9, the ZMNs with high crystallinity and a thickness of 80~100 nm can be synthesized successfully, whatever inorganic or organic acids are used to regulate the pH of aging gel to around 8.5, indicating the neglectable influence of anions on S-1 ZMN synthesis. Inorganic cations, particularly alkali metal cations, might possess structure-directing effects and facilitate the formation of zeolites with distinct framework types[41,42]. The influence of cations is also explored in this study, and metal sulfate salts are

selected as the sources of metal ions as they will not change the pH of the gel or introduce any other anions. As shown in Supplementary Figure 10, all samples synthesized in the presence of Li^+, Na^+, K^+, and Mg^{2+} maintain the macro-nanosheet morphology. However, the thickness along the *b*-axis increases from *ca.* 80 to 150~200 nm when Li^+ and Mg^{2+} are present in the synthesis gel, while Na^+ and K^+ have little influence on the thickness along the *b*-axis but slightly promote the growth along the *c*-axis. Obviously, the synthesis method combining aging and pH regulation presented here is robust and rarely influenced by other cations and anions.

Temperature has a significant impact on both zeolite nucleation and crystal growth. Supplementary Figure 11 shows SEM images of the samples synthesized at different crystallization temperatures. The ZMNs are obtained within the temperature range of 90~180 °C, and there is a slight increase in the size of crystals as the crystallization temperature increases. Meanwhile, the corresponding relative crystallinity of the sample synthesized at 90 °C is only 85% of those synthesized at higher temperatures, even though the crystallization has been prolonged from 72 to 96 h. This can be attributed to the promoted crystal growth rate caused by the temperature increase. The temperature has little influence on the S-1 ZMN synthesis, in accordance with our previous report of MFI ZMNs synthesized in fluorine media[26]. In our previous work, the pH of the aging gel is similar to that in this study due to the addition of NH_4F, and the ZMNs with high crystallinity can be synthesized at 90 °C for 72 h. The difference reveals that fluorine shows significant promotion effects on zeolite crystal growth[39], while it has little influence on zeolite nucleation.

Normally, the SDA, namely TPAOH herein, always has a strong impact on MFI zeolite synthesis and zeolite morphology due to the abundant nucleation in TPA-rich systems. In our previous study of MFI ZMNs synthesized in fluorine media, TPAOH content plays a key role in determining the thickness of the ZMN[26]. As expected, the TPAOH content can also reduce the overall S-1 ZMN crystal dimensions, and the thickness of obtained ZMNs decreases from 200 to 50 nm when the TPAOH/SiO_2 ratio increases from 0.1 to 0.3 [Supplementary Figure 12]. However, the reduction effect of TPAOH content is relatively limited under employed conditions, as the thickness of as-synthesized ZMN can be only decreased to ~50 nm, and meanwhile, the crystal edge becomes irregular. This is perhaps due to the weakened interactions between the TPA^+ and the Si species caused by the decreased pH in the absence of fluorine ions.

S-1 ZMN crystallization mechanism

For deep insights into S-1 ZMN synthesis, the evolution of the ZMN with the optimal composition of 1.0 SiO_2 : 0.15 TPAOH : 25 H_2O is investigated. Samples are collected at various stages, including the periods of aging at 90 °C, after pH regulation, and after crystallization at 120 °C for 3, 6, 9, 12, 16, 24, 48, and 72 h. From the XRD patterns [Supplementary Figures 5 and 13], all the samples aged at different times and after pH regulation are amorphous. After crystallization for 6 h at 120 °C, a faint diffraction peak at $2\theta = 23.1°$ emerged, indicating the appearance of the MFI phase. After crystallization for 9 h, five characteristic diffraction peaks corresponding to MFI structures are observed. Thereafter, the crystallization progresses rapidly, and a highly crystalline sample can be obtained after 24 h (crystallization completes within 72 h).

The crystal evolution is monitored by TEM. As shown in Figure 3A, bulky and hard particles with a smooth surface are observed after aging for 12 h. With the addition of H_2SO_4 to regulate the pH to 8.5 and aging at 90 °C for another 12 h, the gel particles gradually dissociate into aggregates of tiny pieces with an irregular shape [Figure 3B]. It confirms that decreasing the pH of the gel leads to the depolymerization of the bulky particles (MFI precursors/nucleus) into tiny ones, which subsequently reorganize into aggregates, in agreement with the results of FTIR [Supplementary Figure 4] and Ar adsorption-desorption isotherms [Supplementary Figure 6]. After crystallization at 120 °C for 6 h, the tiny nanoparticles are preserved and

become more dispersed, although MFI traces have been detected by XRD [Supplementary Figure 13]. Upon extending the crystallization time to 9 h, significant changes in the morphologies of the gel particles are observed as nanoparticles begin to aggregate and form elongated aggregates. Nanosheets subsequently appear, and the SAED patterns show slight spots after 12 h of hydrothermal treatment, indicating the presence of a crystalline phase, though tiny nanoparticles are still present. Notably, the SAED patterns are still scattered even though the nanosheets are well-shaped, suggesting that the whole nanosheet has not crystallized completely. As the crystallization progresses, the number of nanosheets increases along with the depletion of tiny nanoparticles, and more distinct spots in the SAED patterns appear. Actually, after crystallization for 48 h, almost all the gel has transformed into ZMNs, in accordance with the XRD results [Supplementary Figure 13]. Obviously, ZMN crystallization can be considered as an assembly-crystallization process and a nonclassical pathway. In general, the crystallization process is quite similar to that in fluorine media[26], that is, aging to form MFI precursors, regulating pH to depolymerize the bulky particles into tiny ones, aggregating tiny particles to nanosheets and consequently crystallizing into MFI structures.

^{29}Si MAS NMR and FTIR are also employed to identify the intermediates during crystallization. Supplementary Figure 14 shows the ^{29}Si MAS NMR spectra of samples at different synthesis stages. Resonance signals around δ = -90, -100, and -110 ppm are assigned to Q_2 [$(SiO)_2Si(OH)_2$], Q_3 [$(SiO)_3SiOH$], and Q_4 [$Si(SiO)_4$] silicon species, respectively[26,43,44]. After aging and pH regulation, the samples exhibit a high number of Q_3 sites (~50%) and a small number of Q_2 sites (~10%), suggesting the formation of zeolite precursors. Meanwhile, the intensities of Q_3 and Q_2 peaks increase after pH regulation, indicating that the aggregation of MFI zeolite precursors for ZMN synthesis is dissociated to some extent into tiny particles but not dissolved. However, upon entering the crystallization stage, the Q_2 signal peak disappears completely, and the intensity of the Q_3 signal peak significantly decreases, while the intensity of the Q_4 signal peak increases, revealing the amorphous state of the gel at the initial hydrothermal treatment. With the extension of crystallization time, the Q_4 peak continues to increase, indicating the crystallization of the nanosheets, and a new peak around -103 ppm attributed to Q_3 of zeolite framework defect Si species increases. This implies a transformation of amorphous gel to crystallized zeolite nanosheets. Another issue is the Q_3/Q_4 ratio, which increases gradually with the crystallization extension and levels off after 24 h, indicating that more Q_3 (framework defects) than Q_4 are formed, and ZMN crystal growth completes after crystallization for 24 h, in agreement with the XRD results. Meanwhile, the Q_3/Q_4 ratio here over 1/2 is much higher than those synthesized in fluorine media and alkali media, standing for more framework defects in ZMN crystals caused by the assembly-crystallization process.

The FTIR spectra of samples crystallized at different times are presented in Supplementary Figure 15. The bands at 1,100 and 800 cm^{-1} correspond to the asymmetric and symmetric stretching of the Si-O-Si bond, respectively. The band at 970 cm^{-1} is attributed to the stretching mode of Si-OH and is associated with the Q^3 silicon species[37]. The band at 570 cm^{-1} is attributed to small MFI precursors containing typical pentasil 5MR structures, which significantly decrease after pH regulation and almost disappear at the initial hydrothermal treatment. With crystallization time extension, the band around 550 cm^{-1} increases and splits into two bands at 560 and 540 cm^{-1}. It is reported that nano-sized silicalite-1 of 18-100 nm presents a splitting of pentasil vibration into 550 and 570 cm^{-1}[36,45]. Thus, the splitting vibrations at 560 and 540 cm^{-1} can be attributed to the formation of MFI ZMNs with a nano-sized thickness.

The kinetics study of zeolite crystallization is considered to be a practical approach for identifying the nucleation and crystallization mechanisms in zeolite synthesis. The crystallization curves of zeolites in a sigmoidal shape can be fitted with the nonlinear Avrami-Erofeev equation[46-48]. Figure 4A presents the

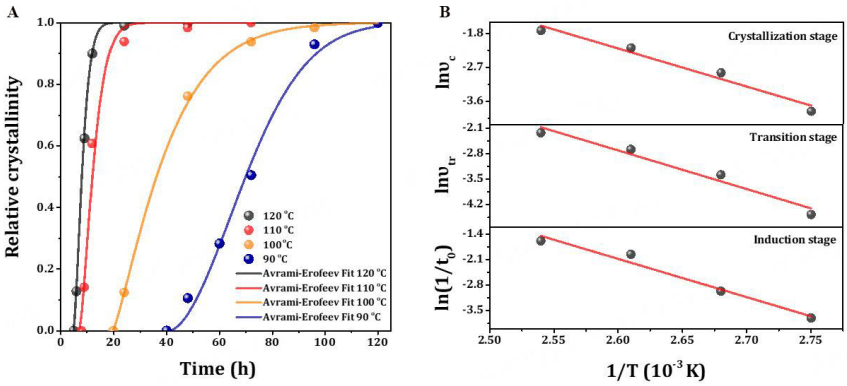

Figure 4. (A) Crystallization curves and (B) Arrhenius plots of crystallization for the S-1 ZMNs synthesized from the system of SiO_2 : 0.15 TPAOH : 25 H_2O and at 90, 100, 110, and 120 °C. TPAOH: Tetrapropylammonium hydroxide; ZMNs: zeolite macro-nanosheets.

crystallization curves of S-1 ZMNs at four different temperatures, which display sigmoidal curves typical for zeolite crystallization and can be distinguished into three stages of crystallization, namely the induction stage, transition stage, and crystal growth stage. With increasing temperature, the whole crystallization time decreases definitely. Table 1 displays the obtained kinetic parameters, calculated by fitting the experimental data. The induction period is longer under lower temperatures and shortened visibly with increasing temperature. For example, at 90 °C, the induction period is 40.5 h, while at 120 °C, it is only 4.9 h. Once the induction period finishes, the crystal growth enters into the transition period, characterized by slow crystal growth. Mintova *et al.* have defined the transition period clearly and separated it into nucleation and crystallization, compensating for the physical limitations involved in characterizing the nucleation rate[46]. An abrupt change in slope observed in crystallization curves indicates that crystals enter a period of rapid growth. The growth rates of the transition (v_{tr}) and crystallization (v_c) stages, as well as the kinetic constant *k*, are accelerated with increasing temperature. Nevertheless, the Avrami exponent n remains constant at approximately 1.6 across the temperature range studied, where n is the sum of two other constants: the number of steps in the nucleation process (δ) and the dimension of crystal growth (ξ)[46,47]. ξ is an integer varying from one to three, representing one-, two-, and three-dimensional growth, respectively, and δ corresponds to different types of nuclei, i.e., zero for instantaneous nucleation and one for continuous nucleation. As a long aging treatment is performed for nucleation, which is considered to be completed at the initial hydrothermal treatment, the δ is defined as zero here. Thus, the n value of approximately two represents a 2D growth process, which increases with decreasing crystallization temperature, implying that the 2D growth should be the intrinsic behavior of our synthesis system and can be promoted by lowering the temperature.

The values of the activation energy (*E*) and pre-exponential factor (ln*A*) for the induction, transition, and crystallization stages of the ZMN synthesis can be calculated from the logarithmic plot of the growth rate versus the reciprocal of the temperature [Figure 4B], which are listed in Table 1. It can be inferred that the induction stage consumes more energy than the growth stage, which should be the rate-determining step of the crystallization process and can be greatly shortened by increasing temperature.

Synthesis of heteroatom-containing MFI ZMNs

The introduction of heteroatoms (including Al) into the neutral framework of pure silicon zeolites can produce Brønsted and Lewis acid sites on the surface of zeolites, endowing zeolites with desired catalytic performance. Therefore, heteroatom-containing MFI ZMNs are synthesized using the strategy developed. The first under consideration is Al-MFI ZMNs, namely ZSM-5 ZMNs. As shown in Supplementary Figures

Table 1. Kinetic parameters of the S-1 ZMNs synthesized from the system of SiO_2 : 0.15 TPAOH : 25 H_2O and crystallized at different temperatures

T (°C)	k (h^{-n})	n	Induction stage	Transition stage		Crystallization stage	
			t_0 (h)	t_{tr} (h)	υ_{tr} (h^{-1})	t_c (h)	υ_c (h^{-1})
120	0.115	1.52	4.9	5.3	0.107	6.5	0.176
110	0.0629	1.48	7.1	7.6	0.0681	9.4	0.111
100	0.0172	1.60	19.3	20.8	0.0339	24.5	0.0578
90	0.0012	1.85	40.5	47.1	0.0114	57.6	0.0209
E (kJ/mol)			90.41	88.06		83.69	
ln$A$			25.21	24.82		23.96	

TPAOH: Tetrapropylammonium hydroxide; ZMN: zeolite macro-nanosheet.

16 and 17, ZSM-5 ZMNs with Si/Al = 100 and a thickness of 90-100 nm along the *b*-axis have been successfully synthesized. The TEM mapping images reveal that Al species are uniformly dispersed in the ZMN crystal without agglomeration. The ^{27}Al MAS NMR spectrum shows a dominant signal located at ~56 ppm attributed to the tetrahedrally coordinated framework Al and no signal at ~0 ppm can be observed, indicating the absence of extra-framework Al species. The catalytic performance of ZSM-5 ZMNs was evaluated in the methanol-to-hydrocarbon (MTH) reaction, and the results were shown in Supplementary Figure 18. ZSM-5 ZMNs exhibit a lifetime of more than 100 h (methanol conversion > 99%), which is longer than the lifetime of commercial ZSM-5 nanocrystals (*ca.* 50 h) in the previous work at completely identical reaction conditions[26]. This could be attributed to the shortened diffusion paths of ZSM-5 ZMNs, which could promote the mass transfer and reduce the coke formation, indicating the potential of ZSM-5 ZMNs as excellent catalysts. Moreover, the selectivity of the ZSM-5 ZMNs (propylene selectivity of ~30% and BTX selectivity of ~14%) is quite similar to that of the same morphology but synthesized at fluoride media in the previous work[26]. Ti-MFI, namely TS-1 ZMNs, has also been successfully synthesized with a thickness of *ca.* 100 nm along the *b*-axis [Figure 5A]. The XRD pattern confirms that the TS-1 ZMN owns MFI topology and high crystallinity [Figure 5B]. The FTIR and UV-vis spectra[Figure 5C and D], which display a band at 960 cm^{-1} and a strong absorbance at ~48,500 cm^{-1}, attributed to the stretching vibration of Si-O-Ti or Si-O perturbed by a Ti atom and tetrahedral-coordinated Ti species (TiO_4) in the framework, respectively[17,49], reveal the existence of framework Ti species. Notably, no band is observed at 38,500 or 30,000 cm^{-1}, indicating that extraframework isolated species and oligomeric Ti species are absent in the as-synthesized TS-1 ZMN[17,49]. Figure 5E displays a TEM image of a single TS-1 ZMN crystal and the corresponding element mapping analyses, showing a Si/Ti ratio close to 72. Obviously, Ti species are evenly distributed in the zeolite framework, and no aggregated particles are present.

CONCLUSIONS

A simple method has been developed for synthesizing MFI zeolite nanosheets by combining aging and following pH regulation in the absence of complex SDA/additives and Fluorine ions. The as-synthesized ZMNs own a thickness of 50~100 nm along the *b*-axis, which can be tuned by the TPAOH dosage, a length of *ca.* 1 μm along the *c*-axis and an almost constant width of 250 nm along the *a*-axis. Thus, the nanometer thickness of ZMNs can shorten the diffusion path and then reduce the diffusion resistance effectively, while its macro single crystal morphology makes it be separated from the synthesis mother liquid just by simple filtration. Moreover, the absence of complex SDA/additives and fluorine ions and crystallization at a relatively low temperature (120 °C) endow the synthesis strategy with remarkably low cost and high eco-friendliness.

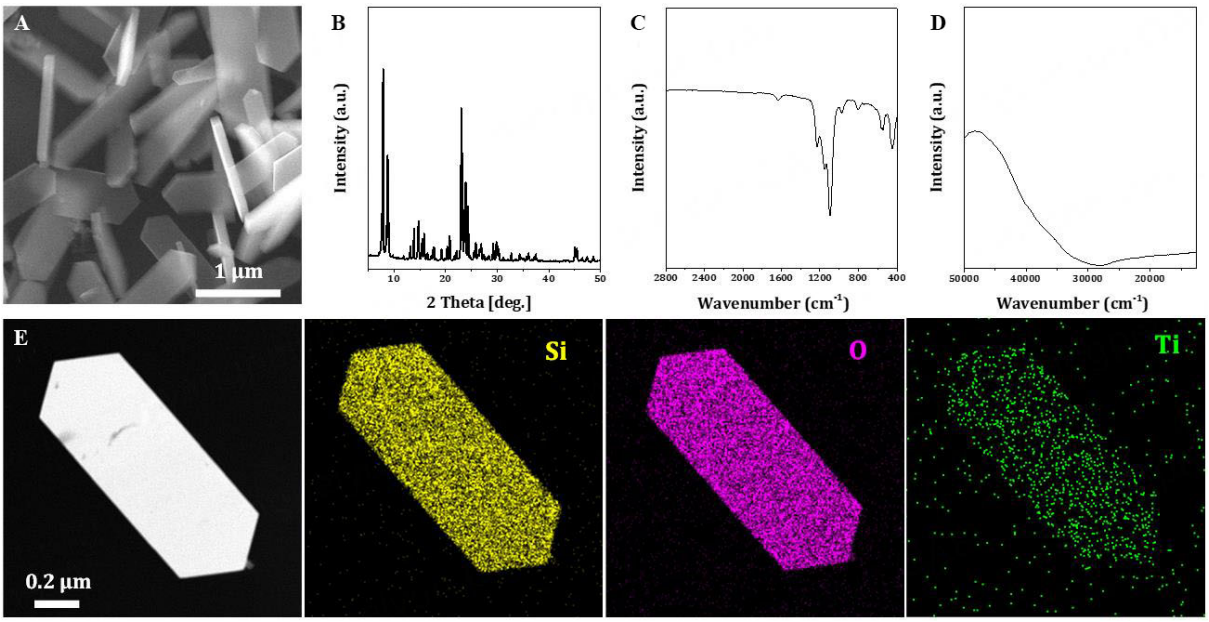

Figure 5. General features of TS-1 ZMN synthesized in the system of 1.0 SiO_2 : 0.15 TPAOH : 0.02 TBOT : 25 H_2O: (A) SEM image and (B) XRD patterns of the as-synthesized TS-1 ZMN; (C) FTIR and (D) DR UV-vis spectra of calcined TS-1 ZMN; and (E) TEM images of a single TS-1 ZMN crystal and corresponding element mapping analyses. FTIR: Fourier transform infrared; SEM: scanning electron microscope; TEM: transmission electron microscopy; XRD: X-ray diffraction; ZMN: zeolite macro-nanosheet.

Aging at a relatively high temperature for an appropriate time (90 °C, 12 h) and low alkalinity (pH = 7.0~8.5) plays crucial roles in MFI ZMN synthesis because the former can promote the formation of sufficient MFI precursors with short-range microporous order, while the latter can dissociate the formed MFI precursors to tiny ones and induce them to undergo oriented aggregation during hydrothermal treatment. The crystallization process exhibits an assembly-crystallization and nonclassical crystallization mechanism, and the oriented growth could be attributed to the intrinsic behavior under the current optimized conditions, as revealed by the crystallization kinetic study.

The above-mentioned synthesis approach is also effective for synthesis of heteroatom-containing MFI ZMNs, such as ZSM-5 ZMN and TS-1 ZMN. We believe that this simple and efficient synthesis method will shed light on both zeolite synthesis and morphology control.

DECLARATIONS

Authors' contributions

Carried out the zeolite preparation and characterization, performed data curation, and prepared the draft manuscript: Tai W

Analyzed the data and provided helpful discussions: Dai W

Directed and supervised the project, analyzed the data, and wrote and revised the manuscript: Wu G

Directed and supervised the project and revised the manuscript: Li L

Availability of data and materials

The data that support the findings of this study are available from the corresponding author upon reasonable request.

Financial support and sponsorship

This work is supported by the National Key R&D Program of China (2021YFA1501202), the National Natural Science Fund of China (22172079), the Municipal Natural Science Fund of Tianjin (21JCYBJC00020), and Tianjin Synthetic Biotechnology Innovation Capacity Improvement Project (TSBICIP-KJGG-009).

Conflicts of interest

All authors declared that there are no conflicts of interest.

Ethical approval and consent to participate

Not applicable.

Consent for publication

Not applicable.

REFERENCES

1. Wang X, Ma Y, Wu Q, Wen Y, Xiao FS. Zeolite nanosheets for catalysis. *Chem Soc Rev* 2022;51:2431-43. DOI
2. Chen LH, Sun MH, Wang Z, Yang W, Xie Z, Su BL. Hierarchically structured zeolites: from design to application. *Chem Rev* 2020;120:11194-294. DOI
3. Choi M, Na K, Kim J, Sakamoto Y, Terasaki O, Ryoo R. Stable single-unit-cell nanosheets of zeolite MFI as active and long-lived catalysts. *Nature* 2009;461:246-9. DOI
4. Na K, Choi M, Park W, Sakamoto Y, Terasaki O, Ryoo R. Pillared MFI zeolite nanosheets of a single-unit-cell thickness. *J Am Chem Soc* 2010;132:4169-77. DOI PubMed
5. Xu D, Ma Y, Jing Z, et al. π-π interaction of aromatic groups in amphiphilic molecules directing for single-crystalline mesostructured zeolite nanosheets. *Nat Commun* 2014;5:4262. DOI
6. Shen X, Mao W, Ma Y, et al. A hierarchical MFI zeolite with a two-dimensional square mesostructure. *Angew Chem Int Ed Engl* 2018;57:724-8. DOI
7. Lu K, Huang J, Ren L, et al. High ethylene selectivity in Methanol-to-Olefin (MTO) reaction over MOR-zeolite nanosheets. *Angew Chem Int Ed Engl* 2020;59:6258-62. DOI
8. Mallette AJ, Seo S, Rimer JD. Synthesis strategies and design principles for nanosized and hierarchical zeolites. *Nat Synth* 2022;1:521-34. DOI
9. Shamzhy M, Gil B, Opanasenko M, Roth WJ, Čejka J. MWW and MFI frameworks as model layered zeolites: structures, transformations, properties, and activity. *ACS Catal* 2021;11:2366-96. DOI
10. Shan Z, Wang H, Meng X, et al. Designed synthesis of TS-1 crystals with controllable b-oriented length. *Chem Commun* 2011;47:1048-50. DOI
11. Yang J, Gong K, Miao D, et al. Enhanced aromatic selectivity by the sheet-like ZSM-5 in syngas conversion. *J Energy Chem* 2019;35:44-8. DOI
12. Ali B, Lan X, Arslan MT, Gilani SZA, Wang H, Wang T. Controlling the selectivity and deactivation of H-ZSM-5 by tuning b-axis channel length for glycerol dehydration to acrolein. *J Ind Eng Chem* 2020;88:127-36. DOI
13. Duan J, Chen W, Wang C, et al. Coking-resistant polyethylene upcycling modulated by zeolite micropore diffusion. *J Am Chem Soc* 2022;144:14269-77. DOI
14. Lv X, Yang M, Song S, et al. Boosting propane dehydrogenation by the regioselective distribution of subnanometric CoO clusters in MFI zeolite nanosheets. *ACS Appl Mater Interfaces* 2023;15:14250-60. DOI
15. Chen X, Yan W, Cao X, Yu J, Xu R. Fabrication of silicalite-1 crystals with tunable aspect ratios by microwave-assisted solvothermal synthesis. *Microporous Mesoporous Mater* 2009;119:217-22. DOI
16. Lupulescu AI, Rimer JD. Tailoring silicalite-1 crystal morphology with molecular modifiers. *Angew Chem Int Ed Engl* 2012;51:3345-9. DOI PubMed
17. Song X, Yang X, Zhang T, et al. Controlling the morphology and titanium coordination states of TS-1 zeolites by crystal growth modifier. *Inorg Chem* 2020;59:13201-10. DOI
18. Zhu P, Wang J, Xia F, Zhang W, Liu H, Zhang X. Alcohol-assisted synthesis of sheet-like ZSM-5 zeolites with controllable aspect ratios. *Eur J Inorg Chem* 2023;26:e202200664. DOI
19. Shang Z, Chen Y, Zhang L, Zhu X, Wang X, Shi C. Plate-like MFI crystal growth achieved by guanidine compounds. *Inorg Chem*

Front 2022;9:2097-103. DOI

20. Shang Z, Chen Y, Zhang L, Zhu X, Wang X, Shi C. Constructing single-crystalline hierarchical plate-like ZSM-5 zeolites with short *b*-axis length for catalyzing MTO reactions. *Inorg Chem Front* 2022;9:1456-66. DOI
21. Zhang X, Liu D, Xu D, et al. Synthesis of self-pillared zeolite nanosheets by repetitive branching. *Science* 2012;336:1684-7. DOI
22. Ma Y, Tang X, Hu J, et al. Design of a small organic template for synthesis of self-pillared pentasil zeolite nanosheets. *J Am Chem Soc* 2022;144:6270-7. DOI
23. Jain R, Chawla A, Linares N, García Martínez J, Rimer JD. Spontaneous pillaring of pentasil zeolites. *Adv Mater* 2021;33:e2100897. DOI PubMed
24. Liu Y, Ji T, Zhou T, Lu J, Li H, Liu Y. Preparation of MFI nanosheets with distinctive microstructures via facile alkaline etching. *Ind Eng Chem Res* 2021;60:16296-303. DOI
25. Zhou T, Zhang D, Liu Y, et al. Construction of monodispersed single-crystalline hierarchical ZSM-5 nanosheets via anisotropic etching. *J Energy Chem* 2022;72:516-21. DOI
26. Dai W, Kouvatas C, Tai W, et al. Platelike MFI crystals with controlled crystal faces aspect ratio. *J Am Chem Soc* 2021;143:1993-2004. DOI PubMed
27. Dai W, Zhang L, Liu R, Wu G, Guan N, Li L. Plate-like ZSM-5 zeolites as robust catalysts for the cracking of hydrocarbons. *ACS Appl Mater Interfaces* 2022;14:11415-24. DOI PubMed
28. Zhang L, Yang L, Liu R, et al. Design of plate-like H[Ga]MFI zeolite catalysts for high-performance methanol-to-propylene reaction. *Microporous Mesoporous Mater* 2022;333:111767. DOI
29. Dai W, Ruaux V, Deng X, et al. Synthesis and catalytic application of nanorod-like FER-type zeolites. *J Mater Chem A* 2021;9:24922-31. DOI
30. Wang Z, Zhang H, Ma Y, et al. Transfer printing platelike MFI crystals as seeds for the preparation of silicalite-1 membranes. *Microporous Mesoporous Mater* 2022;336:111895. DOI
31. Hedlund J, Zhou M, Faisal A, et al. Controlling diffusion resistance, selectivity and deactivation of ZSM-5 catalysts by crystal thickness and defects. *J Catal* 2022;410:320-32. DOI
32. Zhang J, Ren L, Zhou A, et al. Tailored synthesis of ZSM-5 nanosheets with controllable *b*-axis thickness and aspect ratio: strategy and growth mechanism. *Chem Mater* 2022;34:3217-26. DOI
33. Zhang J, Zhou A, Gawande K, et al. *b*-Axis-oriented ZSM-5 nanosheets for efficient alkylation of benzene with methanol: synergy of acid sites and diffusion. *ACS Catal* 2023;13:3794-805. DOI
34. Peng Y, Lu X, Wang Z, Yan Y. Fabrication of *b*-oriented MFI zeolite films under neutral conditions without the use of hydrogen fluoride. *Angew Chem Int Ed Engl* 2015;54:5709-12. DOI
35. Kumar S, Wang Z, Penn RL, Tsapatsis M. A structural resolution cryo-TEM study of the early stages of MFI growth. *J Am Chem Soc* 2008;130:17284-6. DOI PubMed
36. Lesthaeghe D, Vansteenkiste P, Verstraelen T, et al. MFI fingerprint: how pentasil-induced IR bands shift during zeolite nanogrowth. *J Phys Chem C* 2008;112:9186-91. DOI
37. Hsu CY, Chiang AS, Selvin R, Thompson RW. Rapid synthesis of MFI zeolite nanocrystals. *J Phys Chem B* 2005;109:18804-14. DOI PubMed
38. Shi D, Haw KG, Kouvatas C, et al. Expanding the synthesis field of high-silica zeolites. *Angew Chem Int Ed Engl* 2020;59:19576-81. DOI
39. Qin Z, Lakiss L, Tosheva L, et al. Comparative study of nano-ZSM-5 catalysts synthesized in OH^- and F^- Media. *Adv Funct Mater* 2014;24:257-64. DOI
40. Ma Q, Fu T, Ren K, Li H, Jia L, Li Z. Controllable orientation growth of ZSM-5 for methanol to hydrocarbon conversion: cooperative effects of seed induction and medium pH control. *Inorg Chem* 2022;61:13802-16. DOI
41. Hikichi N, Iyoki K, Naraki Y, et al. Role of sodium cation during aging process in the synthesis of LEV-type zeolite. *Microporous Mesoporous Mater* 2019;284:82-9. DOI
42. Luo D, Wang Q, Fan D, et al. Hydrothermal synthesis of siliceous beta zeolite by an inorganic cation-driven strategy and its crystallization mechanism. *Microporous Mesoporous Mater* 2022;329:111557. DOI
43. Grand J, Talapaneni SN, Vicente A, et al. One-pot synthesis of silanol-free nanosized MFI zeolite. *Nat Mater* 2017;16:1010-5. DOI
44. Sheng Z, Li H, Du K, et al. Observing a zeolite nucleus (subcrystal) with a uniform framework structure and its oriented attachment without single-molecule addition. *Angew Chem Int Ed Engl* 2021;60:13444-51. DOI
45. Zecchina A, Bordiga S, Spoto G, et al. Silicalite characterization. 1. Structure, adsorptive capacity, and IR spectroscopy of the framework and hydroxyl modes. *J Phys Chem* 1992;96:4985-90. DOI
46. Mintova S, Valtchev V, Vultcheva E, Veleva S. Crystallization kinetics of zeolite ZSM-5. *Zeolites* 1992;12:210-5. DOI
47. Uzcátegui D, González G. Study of the kinetics of crystallization of zeolite MEL. *Catalysis Today* 2005;107-8:901-5. DOI
48. Kadja GTM, Azhari NJ, Mukti RR, Khalil M. A mechanistic investigation of sustainable solvent-free, seed-directed synthesis of ZSM-5 zeolites in the absence of an organic structure-directing agent. *ACS Omega* 2021;6:925-33. DOI PubMed PMC
49. Xu W, Zhang T, Bai R, Zhang P, Yu J. A one-step rapid synthesis of TS-1 zeolites with highly catalytically active mononuclear TiO_6 species. *J Mater Chem A* 2020;8:9677-83. DOI